Exhaust Gas Flowfield from the Deflection of Twin Jets

STEPHEN B. DUNKELBERG,* RALPH T. FAGAN,† AND WARREN A. GISS‡
General Dynamics Corporation, Fort Worth, Texas

The aft engine placement, over-all length, and nose-tow catapulting provisions of the F-111B result in engine nozzle to jet blast deflector clearances that are appreciably less than those existing with current operational aircraft. An analytic and test program was conducted to determine the temperature field and heat transfer resulting from this deflection of jet engine exhaust. The analysis and test showed that a strong forward flow of engine exhaust gas existed. Test results were obtained to define the effect of engine-blast deflector separation and blast deflector skew angle on the temperature field, for situations modeling the F-111B relationship to existing blast-deflector designs. Comparative tests of alternate deflector designs showed that a supplementary deflector can minimize the forward flow of hot exhaust gases. Heat-transfer coefficient data were obtained for representative locations on the airplane for the most severe conditions expected with current deflector designs.

Nomenclature

A = area enclosed by angle $d\omega$ (Fig. 2)
a = distance from stagnation point or stream tube up to the edge of the jet (Fig. 2)
b = distance from stagnation point or stream tube down to the edge of the jet (Fig. 2)
c = heat capacity
D = characteristic length
h = heat-transfer coefficient
k = thermal conductivity
M, dM = momentum
m = mass flow rate
S = stagnation point or stagnation stream tube
T = gas temperature recorded during model test; also subscripted as T_{amb}, T_j
V = velocity: unsubscripted to show model-test data; subscripted as V_1, V_2, V_a, V_b for analysis; subscripted as V_j for model-test jet velocity
X = distance from the model centerline, measured horizontally, perpendicular to model centerline
Y = distance forward of the JBD, measured horizontally, parallel to model centerline
Y_D = distance from nozzle exit to base of the deflector
Z = distance measured vertically above the deck
α = turning angle for a differential element of flow
θ = JBD-deck intersection angle; dimensionless temperature
ρ = density
ϕ = angle from jet vertical centerline, measured in the plane of the deflector
ω = angle from undeflected jet vertical centerline, measured in a plane perpendicular to the jet centerline

Subscripts and superscripts

a = flow that is upward from the stagnation point ($m_{a\phi}$)
amb = ambient
b = flow which is downward from the stagnation point ($m_{b\phi}$)
j = jet (T_j, V_j)
ϕ = the deflected jet at angle ϕ from the vertical centerline (Fig. 2)
ω = the undeflected jet at angle ω from the vertical centerline (Fig. 2)
1 = conditions prior to deflection
2 = conditions after deflection
(′) = full-scale conditions (T_j', V')

Introduction

A JET blast deflector (JBD) is used on aircraft carriers to protect other aircraft, equipment, and personnel from the hot exhaust blast of jet-powered aircraft. A JBD is normally placed behind each catapult, and is raised so that an airplane can set maximum power prior to a catapult launch. The standard JBD design intersects the deck at a 60° angle, is 8 ft in slant height, and is perpendicular to the catapult centerline. The relation of the F-111B to a typical JBD is shown in Fig. 1.

The General Dynamics F-111B is powered by two Pratt & Whitney Aircraft TF30 engines, located in the aft portion of the fuselage. The engine nozzles are virtually the aftmost portion of the airplane, and are spaced 1.6 diam (64 in.) apart. Under the most adverse conditions with present jet blast deflector designs, the engine nozzle exits are 1.175 diam (47 in.) from the deflector, measuring from the nozzle exit plane horizontally to the JBD-deck intersection (distance Y_D in Fig. 1). It was felt that this proximity might have adverse temperature effects, but no literature was found which could be used to predict the environment. The literature did suggest the test methods and data-analysis techniques used in this program.

The temperature field of a single, undeflected jet is treated in Ref. 1, and dual undeflected jets are treated in Ref. 2. The impingement of dual jets on a ground plane is treated in Ref. 3, but the maximum angle considered is 20°. Reference 4 considers deflection angles up to 50°, but for a single jet, and investigated only in the direction of anticipated flow. This paper shows that there was a smaller flow in the opposite direction which was not investigated.

Theoretical Flowfield

Location of the stagnation point of a single jet impinging on a flat plate will depend on the turning angle, and can be determined from a momentum balance of the streams leaving

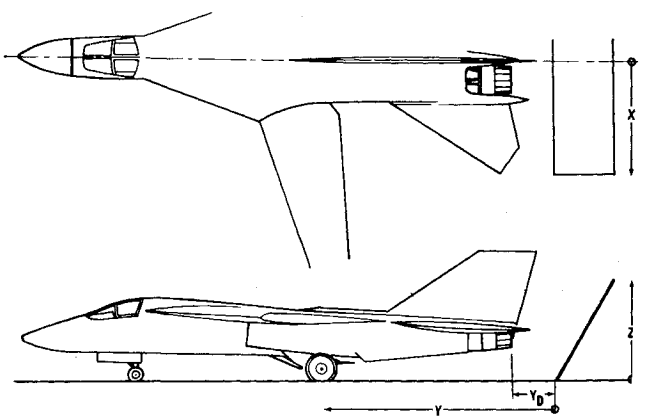

Fig. 1 F-111B—jet blast deflector relationship.

Received July 11, 1966; revision received April 5, 1967. [3.01, 4.01]

* Project Aerothermodynamics Engineer.
† Senior Aerothermodynamics Engineer.
‡ Aerothermodynamics Engineer.

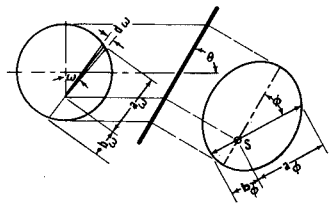

Fig. 2 Coordinates in the undeflected jet cross section and projected on the JBD plane.

the stagnation point. To determine the stagnation point and flow division, it is assumed that there are no losses in turning. Thus, isentropic stagnation pressure exists at the stagnation point, and, where turning is complete, velocity is equal to incident velocity.

The division of flow between the a_ϕ and b_ϕ directions, as defined in Fig. 2, depends on the cosine of the actual turning angle. To determine the actual turning angle, consider Fig. 3. The actual turning angle for flow toward a_ϕ is α, and for flow toward b_ϕ it is $(180 - \alpha)$. It can be shown that

$$\cos\alpha = \cos\theta \cos\phi \tag{1}$$

$$\cos(180 - \alpha) = -\cos\theta \cos\phi \tag{2}$$

For a stream turned by either blade or aerodynamic forces, there must be a balance of forces with momentum change. Consider coordinates in a plane containing the stagnation stream tube and inclined at angle ϕ to include a_ϕ and b_ϕ. This is shown in Fig. 4, with $x+$ in the direction of a_ϕ. All momentum changes in the y direction will be balanced by pressure forces on the deflecting surface. Momentum changes in the $x+$ direction must be balanced by corresponding momentum changes in the $x-$ direction. These are

$$x+: \quad dM_{a_2} - dM_{a_1} = dm_{a\phi}V_1 - dm_{a\phi}V_1\cos\alpha = dm_{a\phi}V_1(1 - \cos\theta\cos\phi) \tag{3}$$

$$x-: \quad dM_{b_2} - dM_{b_1} = dm_{b\phi}V_1(1 + \cos\theta\cos\phi) \tag{4}$$

and since these momentum changes must balance,

$$dm_{a\phi}/dm_{b\phi} = (1 + \cos\theta\cos\phi)/(1 - \cos\theta\cos\phi) \tag{5}$$

Considering the cross section of the undeflected jet (Fig. 2), a differential angle $d\omega$ contains the mass $dm_{a\phi}$ which will be deflected in the direction a_ϕ. The cross-section area bounded by this angle is

$$dA_\omega = \tfrac{1}{2}a_\omega^2 d\omega \tag{6}$$

and by continuity the mass is

$$dm_{a\phi} = \tfrac{1}{2}\rho V_1 a_\omega^2 d\omega \tag{7}$$

since

$$a_\omega = a_\phi \sin\alpha \tag{8}$$

$$dm_{a\phi} = \tfrac{1}{2}\rho V_1 a_\phi^2 \sin^2\alpha\, d\omega \tag{9}$$

Similarly,

$$dm_{b\phi} = \tfrac{1}{2}\rho V_1 b_\phi^2 \sin^2\alpha d\omega \tag{10}$$

and by solving (9) and (10) for $\frac{1}{2}\rho V_1 \sin^2\alpha$ and equating,

$$dm_{a\phi}/dm_{b\phi} = a_\phi^2/b_\phi^2 \tag{11}$$

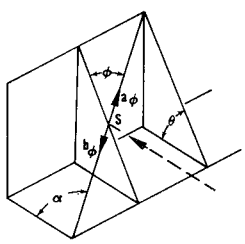

Fig. 3 Schematic definition of angles used for flow deflection.

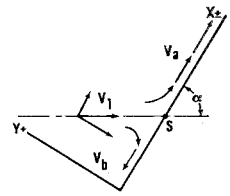

Fig. 4 Coordinate system for momentum balance.

This is then combined with (5), which gives the relationship

$$a_\phi^2/b_\phi^2 = (1 + \cos\theta\cos\phi)/(1 - \cos\theta\cos\phi) \tag{12}$$

For $\phi = 0°$ (vertical centerline of the jet),

$$a_\phi/b_\phi = [(1 + \cos\theta)/(1 - \cos\theta)]^{1/2} \tag{12a}$$

At $\phi = 90°$ (horizontal centerline),

$$a_\phi/b_\phi = [(1 + 0)/(1 - 0)]^{1/2} = 1.0 \tag{12b}$$

Thus, the stagnation point is located on the vertical centerline of the impingement zone, at a point determined by the deflector angle.

For a single jet impingement, the deflected flow is in all directions and is rapidly dissipated. For twin-jet impingement, however, the deflected flows of the inboard portion of the jets reinforce one another, as shown on Fig. 5. Here, as previously, the flow direction after the deflected streams from the two jets meet could be determined by a momentum balance. On the line between stagnation points, where there is no x velocity component (per Fig. 4 coordinates), the streams meet and are turned to flow perpendicular to the deflector plane. Above this line, the streams have the same velocity, but with a "plus x" component. Below this line, the flows have a "minus x" component, and the augmented flow is forward. Figure 5 also shows the carrier situation, in which this flow is further deflected by the deck plane. The flows that reach the JBD-deck intersection before reaching the centerline are deflected to flow forward and inboard. The result is that a major portion of the jets (i.e., that which is inboard of and below the stagnation points) is focused into an energetic stream that flows forward beneath the airplane fuselage.

The stream division obtained here is only approximate, since there is pressure loss associated with each deflection. However, the geometry obtained is useful in estimating the ratio of forward-inboard flow to total flow. The forward-inboard flow from each jet is proportional to one-half of the area of a segment of the cross section of the jet. This area, shown cross hatched in Fig. 5, is bounded by vertical and horizontal lines drawn through the stagnation stream tube. The ratio of this area to the total area of the two jets is shown

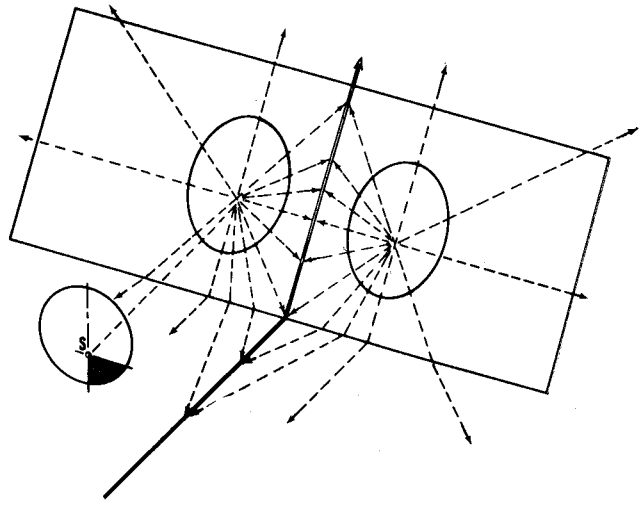

Fig. 5 Schematic of deflected flow paths.

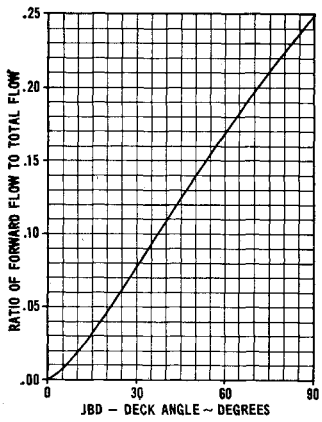

Fig. 6 Effect of jet blast deflector angle on forward flow.

in Fig. 6. This figure shows that for the typical 60° deflector, approximately 17% of the total jet exhaust will be focused into a forward-flowing stream.

Test Program

The test program was designed to measure the effect of the deflected jet on airplane environment and to investigate changes in deflector design that could be made to improve the airplane environment. The test apparatus, shown in Fig. 7, consisted of a $\frac{1}{12}$-scale model of the F-111B aft fuselage, a deck plane, and a jet blast deflector. The aft fuselage was formed from two 4.5-in.-o.d. pipes, which supplied hot, high-pressure air to detailed models of the TF-30 engine nozzles.

Accurate nozzle models were considered essential since the TF30 engine exhaust nozzle was expected to have a significant effect on the flowfield. The engine nozzle, shown schematically in Fig. 8, consists of a conventional primary nozzle and a variable-geometry, ejector-shroud secondary nozzle. Six blow-in doors, located near the plane of the primary nozzle, allow pumping of ambient air if internal pressure is less than ambient pressure. The exit diameter of the secondary nozzle is also determined by a balance of internal and external pressure. Under ground static conditions, the secondary shroud internal pressures are low, the secondary nozzle exit is at minimum diameter, and the blow-in doors are open. This nozzle configuration is shown by the solid lines of Fig. 8, with the dotted lines showing the extreme positions of the nozzle under high internal pressure conditions.

The JBD model used for the majority of the tests was typical of current carrier installations. It intersected the deck plane at a 60° angle, and could be adjusted to vary the airplane-JBD separation and the angle of the JBD to the airplane centerline. Modifications to this deflector design

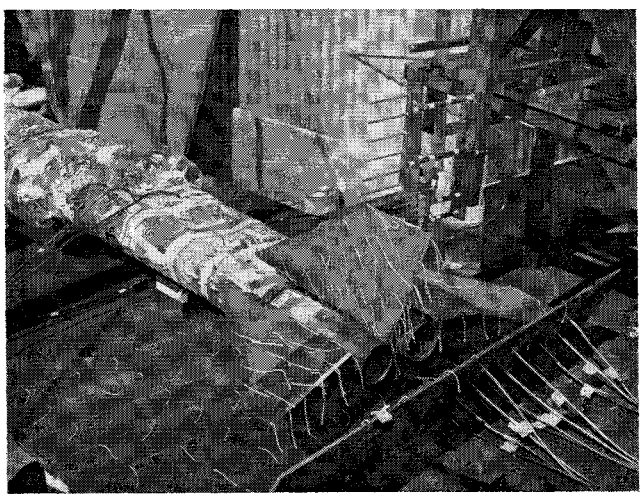

Fig. 7 F-111B JBD model configuration.

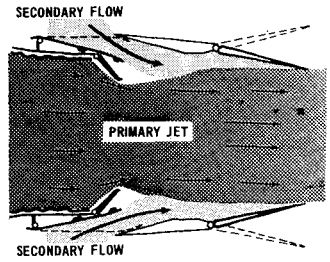

Fig. 8 Schematic of TF30 engine nozzle.

which were tested were as follows: 1) the angle of the JBD to the deck was changed to 45°; 2) a 2.2- × 10-ft supplementary deflector ("fence") was installed 2.2 ft forward of the 60° deflector, at an angle of 60° to the deck; and 3) the fence was retained as in the previous test, and the JBD-deck angle was reduced to 45°.

The modified deflectors were not adjustable in airplane-JBD separation or intersection angle with the airplane centerline. These tests were run at minimum nozzle-JBD distance and at 90° intersection angle, since the previous tests had shown conclusively that this was the worst case.

For the temperature field tests, an 11-point movable thermocouple rake was used (visible in Fig. 7) to measure gas temperature at eight locations in 2-in. increments parallel to the model centerline and at ten locations in 2-in. increments of distance from the centerline. A total of 880 temperatures were possible for each test, but readings were discontinued in both directions when all thermocouples indicated ambient temperature. Temperature field data were recorded only for the basic 60° deflector model, since the modified deflectors were not compatible with the traversing rake. Gas temperature at five locations on the model—corresponding to the location of engine inlets, main landing gear, and three points on the aft fuselage lower surface—was recorded during all tests.

Figures 9 through 13 show typical results of the temperature field tests. In these figures, the measured temperatures have been reduced to nondimensional terms by the relationship

$$\theta = (T - T_{\text{amb}})/(T_j - T_{\text{amb}}) \qquad (13)$$

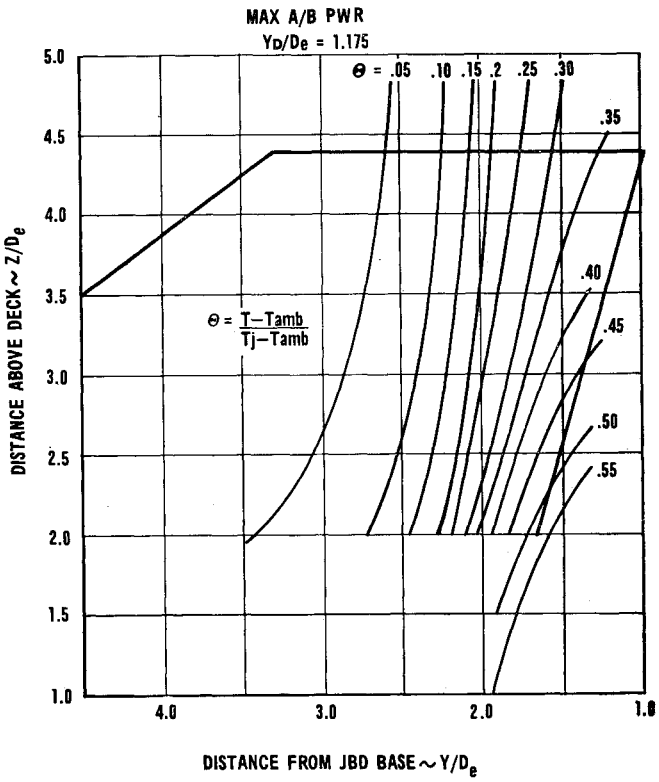

Fig. 9 Gas temperatures on the vertical stabilizer.

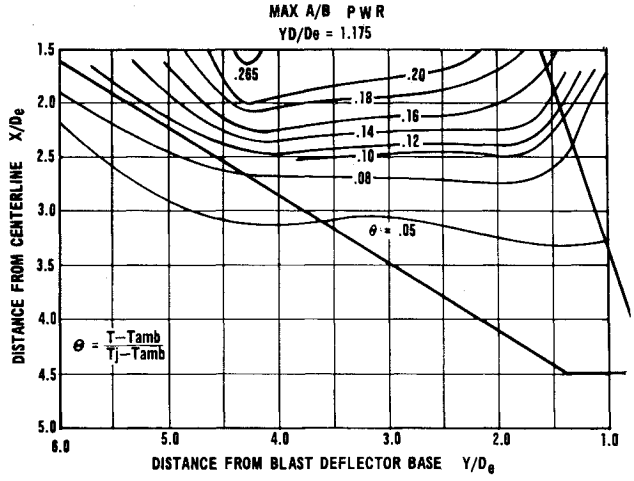

Fig. 10 Gas temperatures on the horizontal stabilizer lower surface.

Distances in these figures are shown in terms of secondary nozzle diameters, and are measured as shown in Fig. 1. For all tests, the nozzle centerlines were 1.39 diam above the deck and inclined downward at 3.5°.

Figures 9, 10, and 11 show gas temperature field data obtained at the minimum nozzle-JBD distance and for maximum afterburner power. Figure 9 shows the temperature field on the vertical tail. Figure 10 shows the temperature field on the lower surface of the horizontal tail. Figure 11 shows the temperature field at the deck. The effect of nozzle-JBD separation is shown by Figs. 12 and 13. Figure 12 shows gas temperature at five levels on the vertical tail as a function of nozzle-JBD distance. Figure 13 shows temperatures from five locations on the fuselage as a function of nozzle-JBD distance.

Flowfield visualization was accomplished by tufts attached to the fuselage, deck, and deflector; by a tufted wand; and (serendipitously) by water accumulated in the air supply lines. Figures 14–17 show typical results. Figures 14 and 15 show tuft patterns for angles of the JBD to the model centerline of 90° and 84°, respectively. These figures illustrate the energetic forward flow on the deck, the flow pumped by the ejector nozzle, and the strong upward flow along the trailing edge of the vertical stabilizer. Figure 15 also shows that for the 84° case the forward flow is spilled to the open side of the deflector, leaving the tufts under the fuselage undisturbed. Figure 16 shows the pattern formed

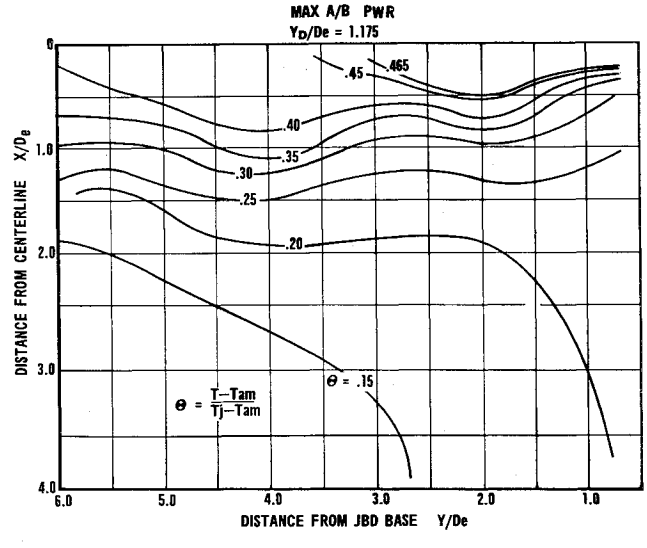

Fig. 11 Gas temperatures on the deck.

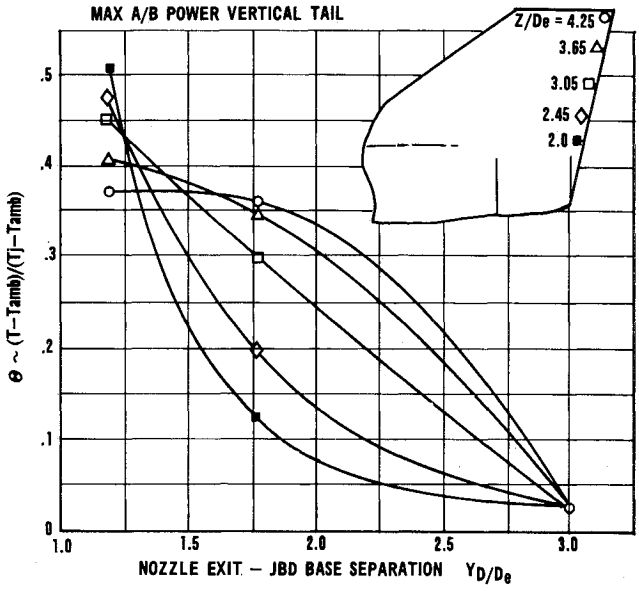

Fig. 12 Effect of nozzle-JBD separation on vertical stabilizer gas temperatures.

on the JBD by water entrained in the air supply, and was included for comparison to Fig. 5. Figure 17 is a schematic of the flowfield found around the horizontal stabilizer and also that directed at the vertical stabilizer. This figure was prepared from observations of the tuft grids and explorations with the tufted wand.

Heat-transfer coefficients on the model were determined by a heat-balance technique, using electrically heated calorimeters. Calorimeter temperature, gas temperature, and heater power were recorded. The heat-balance calculation accounted for heat loss to the model by conduction. Local velocities were also measured, and these velocities were used to calculate heat-transfer coefficients. Full-scale heat-transfer coefficients were determined from both methods, using the turbulent, flat plate equation[5]

$$h = 0.0296 \frac{\rho V c_p}{[V_\rho D/\mu]^{0.2}[C\mu/K]^{2/3}} \qquad (14)$$

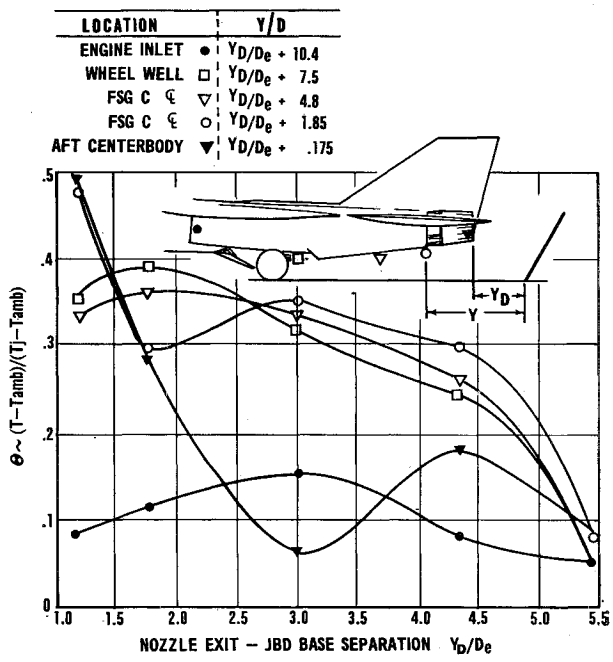

Fig. 13 Effect of nozzle-JBD separation on gas temperatures at the fuselage centerline.

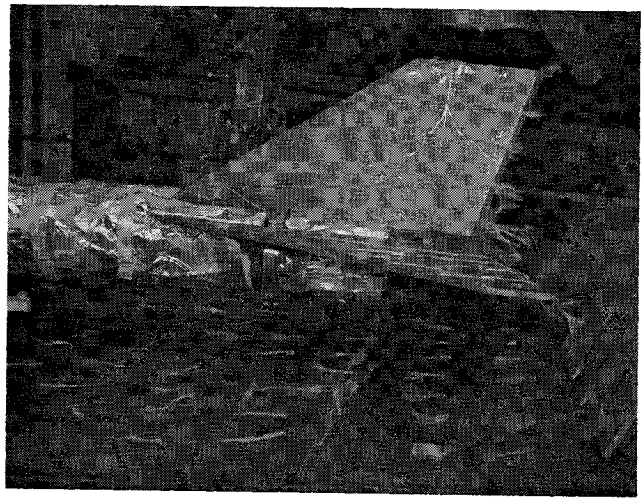

Fig. 14 Tuft patterns for the 60° deflector at 90° to the model centerline.

Full-scale velocity was obtained (as in Refs. 1–4) by the equation

$$V'/V_j' = V/V_j \qquad (V_o = 0) \qquad (15)$$

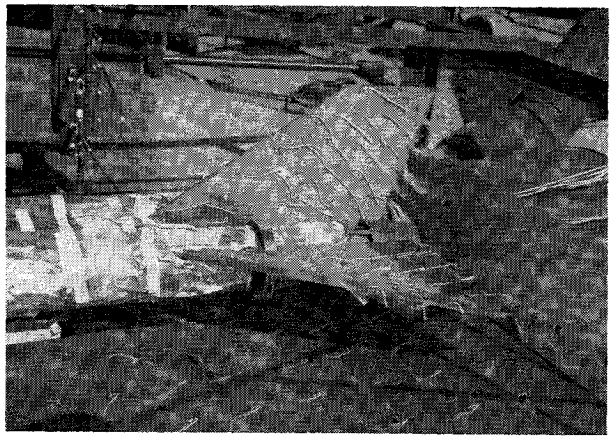

Fig. 15 Tuft pattern for the 60° deflector at 84° to the model centerline.

Since the test conditions duplicated full-scale nozzle pressure ratios, the correction to jet velocity was proportional to the square root of the change in jet temperature, and Eq. (15)

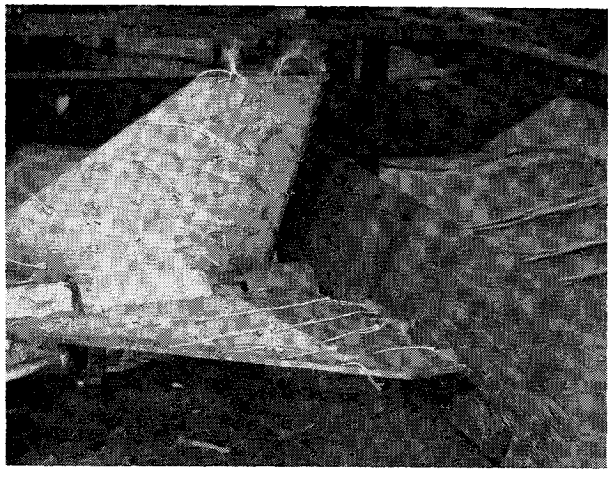

Fig. 16 Water impingement pattern on the 60° deflector at 90° to model centerline.

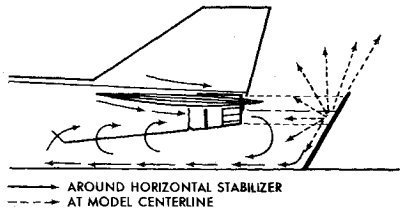

Fig. 17 Schematic of the flowfield at the horizontal stabilizer and at the model centerline.

became

$$V' = V[T_j'/T_j]^{1/2} \qquad (16)$$

Equation (14) was used to determine the ratio of full-scale heat-transfer coefficients to test results. The substitution of Eq. (16) was made for the velocity ratio, and the resulting equation simplified to

$$\frac{h'}{h} = 0.608\left(\frac{T}{T'}\right)^{0.8}\left(\frac{T_j'}{T_j}\right)^{0.4}\left(\frac{C_P'}{C_P}\right)^{1/3}\left(\frac{K'}{K}\right)^{2/3}\left(\frac{\mu}{\mu'}\right)^{0.467} \qquad (17)$$

Table 1 Heat-transfer coefficient test results

	Location				Velocity data			Calorimeter data	
	$\frac{X}{D_e}$	$\frac{Z}{D_e}$	$\frac{Y}{D_e}$	$\frac{Y_D}{D_e}$	V_m	V'	h'	h	h'
Aft	0	1.0	0.8	1.175	...	...	...	84.5	52.2
C'body			1.375	1.75	...	...	...	43.9	29.1
Rudder	0	4.0	1.55	1.175	178	296	20.8	76	51.1
			2.125	1.75	69.4	112	8.47	44.3	29.5
Horizontal stab	1.875	1.2	4.3	1.175	54	90	8.6	30.9	23.5
			4.875	1.75	40	166	9.61	26.0	20.6
Horizontal stab	1.875	1.2	1.36	1.175	91	152	11.4	38.6	29.9
			1.935	1.75	58.6	100	8.81	35.9	29.0

Heat-transfer coefficients from both velocity and calorimeter data are shown in Table 1. There is a wide disagreement, and the calorimeter data are preferred. The extreme turbulence makes the characteristic length of the Reynolds number meaningless, and the velocity measurements were difficult for the same reason.

The temperature and flowfield tests showed that the momentum balance gave a good qualitative description of the

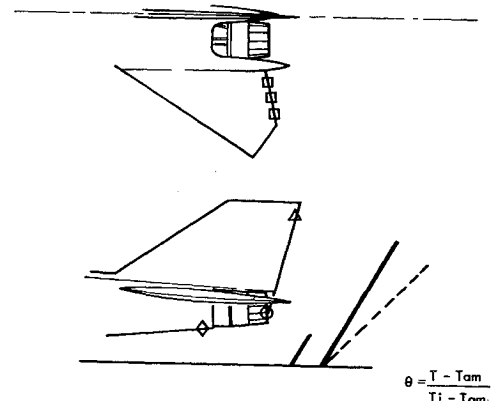

	LOCATION			JBD ANGLE AND CONFIGURATION			
	$\frac{X}{D_e}$	$\frac{Y}{D_e}$	$\frac{Z}{D_e}$	60° NO FENCE	45° NO FENCE	60° 60° FENCE	45° 60° FENCE
△	0	.55	4.25	.372	.109	.424	.046
◇	0	1.35	1.0	.486	.372	.498	.109
◇	0	3.025	~ .8	.465	.431	.063	-0-
□		~1.0	~1.5	.13	(NO DATA)	.294	.029
WHEEL WELL	0	8.7	~ .8	.352	.303	-0-	-0-
ENGINE INLET	0	11.6	~ .8	.088	.121	-0-	-0-

Fig. 18 Effect of JBD modifications on gas temperature.

flowfield and that temperatures could be hazardous to the airplane. The test program was therefore extended to investigate changes in JBD design which might improve the environment. The three configurations described previously, selected as requiring minimum modifications to existing deflectors, were tested. The results of these tests are shown in Fig. 18, with results from the standard deflector included for comparison.

From Fig. 18 it can be seen that these tests successfully demonstrated a JBD design that will prevent any hot gas from reaching the airplane. It can also be seen that modifications which were beneficial in some locations were detrimental in other locations, and that the momentum balance is not adequate to determine the effects of modifications. The fence was expected to turn the forward flow outboard, and (to an extent) it was successful. However, the temperature at the top of the vertical tail shows that the fence also augmented the upward flow. Similarly, reducing the JBD angle to 45° was expected to lower all temperatures on the airplane, but it increased the temperature at the engine inlet.

These test results were valuable in the F-111B program and are generally applicable for situations that duplicate the F-111B nozzle spacing, height above the deck, and nozzle inclination. In any other case, the uncertainties in analysis as demonstrated in this test are such that data from exact models should be obtained.

References

[1] Fleming, W. A., "Characteristics of a hot jet discharged from a jet-propulsion engine," NACA RM E6L27a (1946).

[2] Sloop, J. L. and Morrell, G., "Temperature survey in the wake of two closely located parallel jets," NACA TM E9I21 (1950).

[3] Farmer, J. E., Stepka, F. S., and Garrett, F. B., "Temperature and pressure distribution in dual parallel jets impinging on the ground from a turbojet engine," NACA RM E9L01 (1950).

[4] "Nondimensional characteristics of free and deflected supersonic jets exhausting into quiescent air," Naval Air Development Center Rept. NADC-ED-5401 (1954).

[5] *Aero-Space Applied Thermodynamics Manual* (Society of Automotive Engineers Inc., New York, 1962), p. C-61.

JULY-AUG. 1967 J. AIRCRAFT VOL. 4, NO. 4

Nozzles for Jet-Lift V/STOL Aircraft

J. A. C. KENTFIELD*
Curtiss-Wright Corporation, Wood-Ridge, N. J.

Several types of nozzles for lift and lift/cruise engines are reviewed. Model test data are presented for two types of lift-engine nozzles, one of the short nonvectoring plug type, the other a simple, hemispherical-plug, vectoring nozzle. It was found that the thrust and discharge coefficients obtained with the simple vectoring nozzle were substantially independent of flow-deflection angle. Results of a theoretical analysis are presented which show that attempts to shorten and lighten lift-engine nozzles by eliminating whirl-removing surfaces may incur severe performance penalties. An oblique-joint, elliptical shape nozzle for vectoring lift/cruise engine thrust is described and test data obtained with homogeneous flow are presented. A theoretical analysis was made of the causes of performance loss with nonhomogeneous flow. It was concluded that when a nozzle of this type is employed on a turbofan engine use should be made of an upstream flow mixer, or separate channels to the nozzle exit, if excessive losses are to be avoided in the vectored mode.

Nomenclature

B = bypass ratio
C_D = discharge coefficient; (actual mass flow)/(ideal mass flow for corresponding λ)
C_T = thrust coefficient; (actual thrust for actual mass flow)/(ideal thrust for the same mass flow)
D = maximum engine diameter or major axis of elliptic section
d = minor axis of elliptic section
F = thrust augmentation ratio
M = Mach number
n = number of oblique joints
P = static pressure
P_o = total pressure
P_∞ = ambient pressure
r = radius
X = downward projection or axial length of nozzle
α = ratio; (enthalpy of gas generator flow)/(enthalpy of fan flow)
β = actual flow-deflection angle
β_g = nominal flow-deflection angle based on nozzle geometry
γ = ratio of specific heats
Δ = finite increment
θ = inclination angle of oblique joint
λ = nozzle pressure ratio
ρ = density
φ = flow-discharge angle of truncated plug nozzle
Φ = whirl angle

Subscripts

(AXIAL) = axial component
b = pertaining to base area of truncated plug nozzle
C = cold (fan) flow of a turbofan engine
EQV = circular cross section of equivalent area

Presented at the AIAA Second Propulsion Joint Specialist Conference, Colorado Springs, Colo., June 13–17, 1966 (not preprinted); received October 5, 1966; revision received March 30, 1967. The author wishes to thank the management of the Curtiss-Wright Corporation for permitting the publication of this paper. The efforts of the author's colleagues at the Wright Aeronautical Division who carried out the programming of the flow mixing analysis and assisted in other ways are gratefully acknowledged. The Fluidyne Engineering Corporation of Minneapolis, Minn. obtained the experimental results presented herein under contract from the Curtiss-Wright Corporation. [4.01]

* Project Engineer, Wright Aeronautical Division; now Lecturer, Mechanical Engineering Department, Imperial College, University of London.